AIP | Applied Physics Letters

Quantitative analysis and near-field observation of strong coupling between plasmonic nanogap and silicon waveguides

Rafael Salas-Montiel, Aniello Apuzzo, Cécile Delacour, Zohreh Sedaghat, Aurélien Bruyant et al.

Citation: Appl. Phys. Lett. **100**, 231109 (2012); doi: 10.1063/1.4725511
View online: http://dx.doi.org/10.1063/1.4725511
View Table of Contents: http://apl.aip.org/resource/1/APPLAB/v100/i23
Published by the American Institute of Physics.

Related Articles

Nonlinear response of an ultracompact waveguide Fabry-Pérot resonator
Appl. Phys. Lett. 102, 011133 (2013)

Ultralow VπL values in suspended quantum well waveguides
Appl. Phys. Lett. 101, 241111 (2012)

Ultra-thin silicon-on-insulator strip waveguides and mode couplers
Appl. Phys. Lett. 101, 221106 (2012)

Loop-mirror-based slot waveguide refractive index sensor
AIP Advances 2, 042142 (2012)

Integrated optofluidic index sensor based on self-trapped beams in LiNbO3
Appl. Phys. Lett. 101, 181104 (2012)

Additional information on Appl. Phys. Lett.

Journal Homepage: http://apl.aip.org/
Journal Information: http://apl.aip.org/about/about_the_journal
Top downloads: http://apl.aip.org/features/most_downloaded
Information for Authors: http://apl.aip.org/authors

ADVERTISEMENT

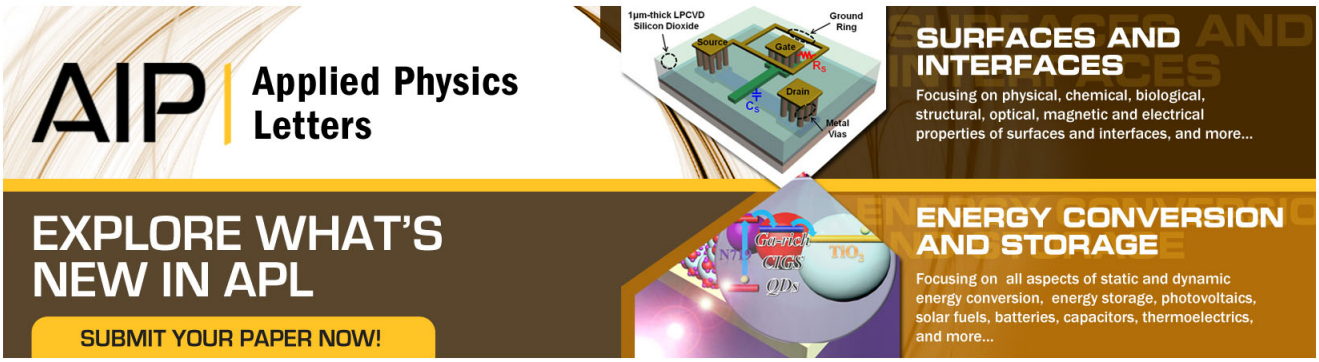

Quantitative analysis and near-field observation of strong coupling between plasmonic nanogap and silicon waveguides

Rafael Salas-Montiel,[1,a)] Aniello Apuzzo,[1] Cécile Delacour,[2,b)] Zohreh Sedaghat,[1] Aurélien Bruyant,[1] Philippe Grosse,[2] Alexei Chelnokov,[2] Gilles Lerondel,[1] and Sylvain Blaize[1,c)]
[1]*LNIO, CNRS UMR 6279, UTT, 12 rue Marie Curie, 10010 Troyes, France*
[2]*CEA Leti Minatec Campus, DOPT, 17 rue des Martyrs, 38054 Grenoble, France*

(Received 1 February 2012; accepted 7 May 2012; published online 6 June 2012)

We present a near field optical study of a plasmonic gap waveguide vertically integrated on silicon. The experimental study is based on a near field scanning optical microscope configured in perturbation mode. This operation mode is described and modeled to give a physical insight into the measured signal. A high spatial resolution allows for the characteristics of the plasmonic gap modes, such as near field distributions, effective indices, direction of propagation, and coupling between perpendicularly polarized modes, to be imaged and analyzed with accuracy. This experimental work is supported by numerical simulations based on finite element optical mode solvers and by the application of the strongly coupled-mode theory to the device. © *2012 American Institute of Physics*. [http://dx.doi.org/10.1063/1.4725511]

Plasmonic structures, such as plasmonic gap waveguides, allow for guiding surface plasmon modes with high confinement and relatively low propagation losses at optical frequencies. The confinement enables a strong enhancement of the electric field inside the nanogap that can be exploited in surface-enhanced spectroscopy,[1] biosensing,[2] and plasmonic nanocircuitry.[3,4] In addition, plasmonic gap waveguides can be further functionalized with active materials such as quantum dots for single quantum emitter applications or loss compensation.[5] Efficient excitation of gap modes has been demonstrated experimentally with the use of nanoantennas[6,7] and tapered silicon waveguides[8] with efficiencies as high as 20% and 35%. More recently, directional coupling between plasmonic gap and silicon waveguides was demonstrated with a coupling efficiency of 60%.[9] Today, with the development of techniques such as electron energy-loss spectroscopy[10] and near field scanning optical microscopy (NSOM), it is possible to study surface plasmon waves such as plasmon gap modes directly.[11,12] For waveguiding structures, collection-mode NSOM (Ref. 13) or photon scanning tunneling microscopy[14] have been used for the direct mapping of local field distributions of surface plasmons. In this work, we use a more convenient NSOM for the measurement of integrated plasmonic structures. It consists of a conventional integrated optics setup and a commercial stand-alone atomic force microscope (AFM) probe. Similar configurations have been applied for the characterization of glass[15] and lithium niobate[16] waveguides as well as on Si-based structures[17,18] and planar microresonators.[19] This technique measures the change in transmission at the device output induced by the AFM probe.[20] Our motivation here is to demonstrate that this configuration is a simple yet powerful technique for the observation and measurement of local electric fields in integrated plasmonic devices.

In order to so, we studied a vertically integrated plasmonic gap waveguide on Si. This experimental work is supported by the theoretical analysis of the device through the finite element optical mode solvers and the strongly coupled mode theory.

The structure, fabricated with standard Si technology at CEA-Leti, is a vertical directional coupler with Si photonics and Cu gap waveguides. Details of the design and fabrication process can be found in Ref. 9. The setup used for the optical near field measurements is an arrangement of a conventional integrated optics setup and a commercial AFM probe set to intermittent mode (Fig. 1). A full description of the setup can be found in Ref. 21.

The surface plasmon gap mode, supported by the copper waveguide (Fig. 2(a)), is efficiently coupled from the Si

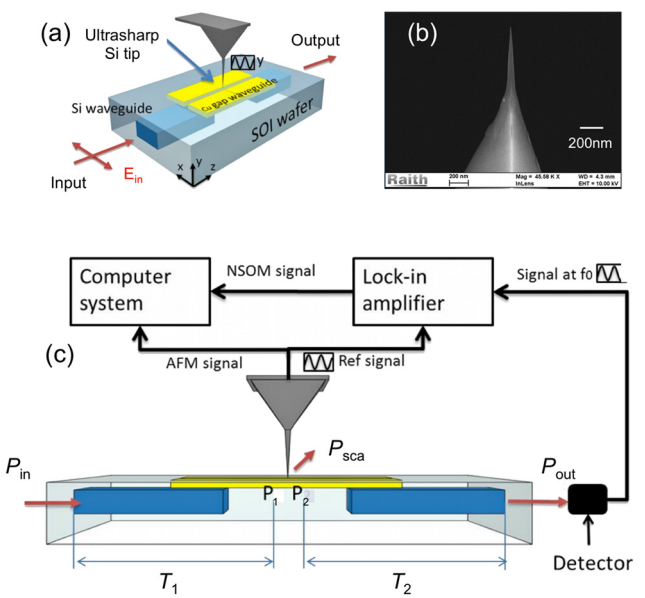

FIG. 1. (a) A 3D artwork of the vertically integrated plasmonic waveguide on Si. (b) SEM image of the AFM probe with a radius of 2 nm. (c) Setup for the measurement of the optical near field.

[a)]Electronic mail: rafael.salas@utt.fr.
[b)]Present address: Institut Néel, 25 av. des Martyrs, 38042 Grenoble.
[c)]Electronic mail: sylvain.blaize@utt.fr.

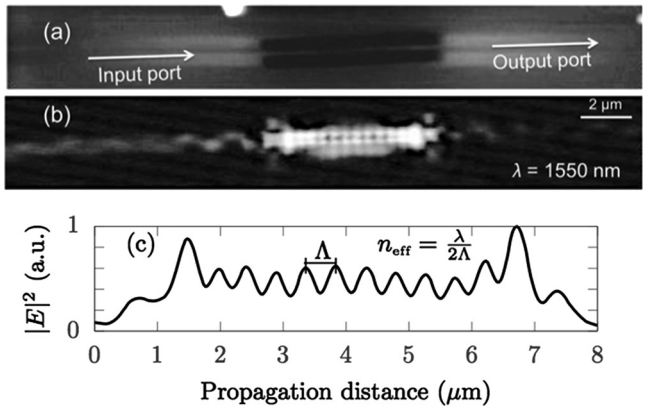

FIG. 2. (a) AFM image showing the surface plasmonic gap waveguide. (b) Optical near field image over the surface of the hybrid structure for an incident quasi-TE fundamental mode at a wavelength of 1550 nm. (c) Standing wave pattern resulting from the interference between the co- and counter-propagating gap modes.

waveguide. This mode propagates through the plasmonic waveguide and is coupled back to output Si waveguide to reach the detector (Fig. 2(b)). The Si waveguide was excited by its fundamental quasi-TE mode at a wavelength of 1550 nm. From the optical image, we plotted a longitudinal profile along the gap waveguide.

Because the AFM probe scans the structure over its surface, only the plasmonic waveguide can be imaged. The optical image shows, however, the incident and transmitted optical modes supported by the Si waveguides. The propagation of the gap mode is clearly seen along the plasmonic waveguide, apparently, without propagation loss. The standing wave pattern, with a period $\Lambda = 460 \pm 60$ nm, can be observed (Fig. 2(c)) as a result of the interference between the co- and counter-propagative gap modes. Modal and propagation characteristics such as effective indices and mode profiles can be obtained by the use of this NSOM in perturbation mode for both waveguides.[21,24] For the Cu gap waveguide, $\beta_2 = \pi/\Lambda = 6.83 \pm 0.22\ \mu m^{-1}$, which is consistent with optical mode solvers calculations.

The efficient excitation of the gap mode is the result of strong coupling between the Si and Cu waveguides as illustrated in Fig. 3. The vertical coupler is excited through the fundamental mode of the single mode Si waveguide. This incident field can be decomposed into the two modes supported by the coupler and propagated through it. After a propagation length (l), the power is transferred to the Cu waveguide. However, not all the power is transferred to the Cu waveguide because of the overlapping between modes of the individual waveguides and because the waveguides have a completely different index profiles.

To investigate the efficiency of the coupler, we have calculated the power transfer efficiency (η) as a function of the separation distance (e) between the two waveguides. The calculations were done using a strongly coupled-mode theory[22,23] valid for lossy systems. The efficiency is defined as the ratio of the optical power at the output of the Cu waveguide to the power at the input of the Si waveguide. The modified propagation constants (γ_a, γ_b) and coupling coefficients (κ_{ab}, κ_{ba}) include the overlap integrals between the fundamental modes of the individual waveguides (C_{ab}, C_{ba}). These four parameters are

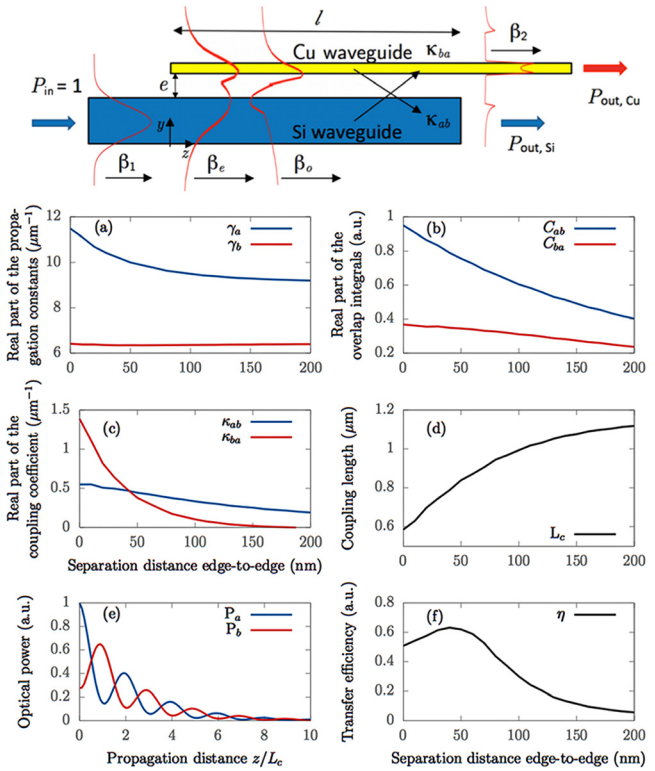

FIG. 3. Strongly coupled waveguides. (a) Calculated propagation constants (γ_a, γ_b), (b) overlap integrals, (c) coupling coefficients, (d) coupling length, and (f) transfer efficiency as a function of the separation distance e. (e) Optical power carried by each waveguide.

$$\gamma_{a,b} = \beta_{1,2} + (\kappa_{11,22} - C \cdot \kappa_{21,12})/(1 - C^2), \quad (1)$$

$$\kappa_{ab,ba} = (\kappa_{12,21} - \kappa_{22,11} \cdot C)/(1 - C^2), \quad (2)$$

where β_1 and β_2 are the propagation constants of the isolated waveguides and κ_{12} and κ_{21} are the conventional coupling coefficients. The parameter C is defined as $C = (C_{ab} + C_{ba})/2$, where $C_{pq} = \frac{1}{2}\int_{-\infty}^{+\infty}[\vec{E}_t^{(q)} \times \vec{H}_t^{(p)}] \cdot \vec{\mathbf{z}}\, dx\, dy$ is the overlap integral coefficient. This coefficient is a measure of the proximity of the waveguides. The four parameters in Eqs. (1) and (2) should include the overlap integral to obtain accurate efficiency results and to satisfy the power conservation law. For maximum power transfer, the coupling length l is chosen such that $\psi l = \pi/2$, where $\psi = (\Delta^2 + \kappa_{ab} \cdot \kappa_{ba})^{\frac{1}{2}}$ and $\Delta = (\gamma_b - \gamma_a)/2$.

The electric and magnetic field distributions of the individual waveguides were calculated with a commercial finite element optical mode solver. The opto-geometrical parameters of the structure were taken from Ref. 9. The results are shown in Fig. 3, where the Si and Cu waveguides are labeled as a and b.

The real part of the propagation constant γ_a decreases as the separation distance e increases. In contrast, γ_b remains almost constant as the separation distance e increases. Therefore, the effects of modal interactions are higher for the propagation constant of the silicon waveguide than that for the copper waveguide for short separation distances e. As expected, the overlapping decreases as the separation distance increases, which leads to a weakly coupled regime.

However, the strong coupling regime is observed with as much as 200 nm of separation between the waveguides ($C_{ab}, C_{ab} \gg 0.1$). For short separation distances ($e < 45$ nm), the coupling coefficient κ_{ba} is higher than κ_{ab}. From this calculation, we can infer that the Si waveguide is strongly perturbed by the presence plasmonic gap waveguide and therefore an efficient coupling can exist. A maximum efficiency is reached at a separation distance of 45 nm, for which $\kappa_{ab} = \kappa_{ba}$. From that separation distance, the efficiency starts to decrease. Looking at a separation distance of 45 nm and a coupling length $L_c = 0.8\,\mu$m, a 60% coupling efficiency is calculated, which is consistent with the measurements already reported in Ref. 9. Finally, the optical power carried by each waveguide, P_a and P_b, is plotted in Fig. 3(e). We observe the power transfer from one waveguide to the other as the propagation distance increase. This transfer decays exponentially as a result of the propagation loss of the plasmonic waveguide.

To interpret the NSOM images (Fig. 2(b)), we present a model of the quantity that is measured by the NSOM in perturbation mode. For that, we inspect each path segment along the structure to obtain the quantity that is measured by the detector (Fig. 1(c)). If we call P_{in} the optical power injected in the waveguiding structure, the optical powers measured just before the probe and at the waveguide output are given by

$$P_1(z_0) = T_1(z_0) \cdot P_{in}, \tag{3}$$

$$P_{out} = T_2(L_t - z_0) \cdot P_2, \tag{4}$$

respectively, where T_1 and T_2 are the power transmission coefficients between the input of the waveguide and the probe located at z_0 and between the probe and the output of the waveguide located at $z = L_t$. By combination of Eqs. (3) and (4), we obtain

$$\frac{P_2(z_0)}{P_1(z_0)} = \frac{P_{out}}{P_{in}} \cdot \frac{1}{T_2(L_t - z_0) \cdot T_1(z_0)}. \tag{5}$$

On the other hand, the optical power immediately after the probe can be written as

$$P_2(z_0) = P_1(z_0) - P_{sca}(z_0), \tag{6}$$

where P_{sca} is the power scattered by the apex of the probe.

By considering that the longitudinal polarizability of the sharp probe apex (y axis) is higher than the polarizability of its transversal components, the expression of P_{sca} can be written as[20]

$$P_{sca} = Q_{\parallel} \frac{1}{2} \sqrt{\frac{\mu_0}{\epsilon_0}} |E_y|^2, \tag{7}$$

where E_y is the y component of the local electric field and $Q_{\parallel}$ is the scattering cross section for the field parallel to the probe axis. The $Q_{\parallel}$ value depends on the probe and sample material geometry and on the local density of radiation modes. The modeling of $Q_{\parallel}$ is therefore a complex problem that in most cases requires tedious numerical calculations.[25] Here, we would like to point out that the probe scatters the y-component of the electrical field more efficiently.

To explicit state the quantity that is measure with this configuration, we can combine Eqs. (5) and (6) to obtain

$$\frac{P_{out}}{P_{in}} = T_2 T_1 \left[1 - \frac{P_{sca}(z_0)}{P_1(z_0)}\right]. \tag{8}$$

From this last equation, it follows that the measured quantity is proportional to the intensity of the local electric field normalized to the guided power flux at z_0. Therefore, an important conclusion is that this NSOM configuration is not convenient for propagation loss measurements along the structure because both P_{sca} and P_1 are expected to decrease in the same ratio.

To confirm our hypothesis that the probe scatters more efficiently the y-component of the electric field than that of the others, we calculated the spatial distribution of the electric field and we analyzed its components with the use of a finite element optical mode solver. We then compared them with the experimental result. To improve the spatial resolution of the optical image (Fig. 2(b)), we rescanned the waveguide with a window scan size of 5 μm by 5 μm and we set the lock-in amplifier to the second harmonic (Fig. 4). Finally, a transversal profile was taken from that image and is plotted as well. The results of the simulations are plotted in Fig. 4.

It is clearly observed in Fig. 4(a) that the calculated electric field power density does not match the measured profile. The calculated power density $|E|^2$ profile is highly confined inside the gap and does not change when the measurement is

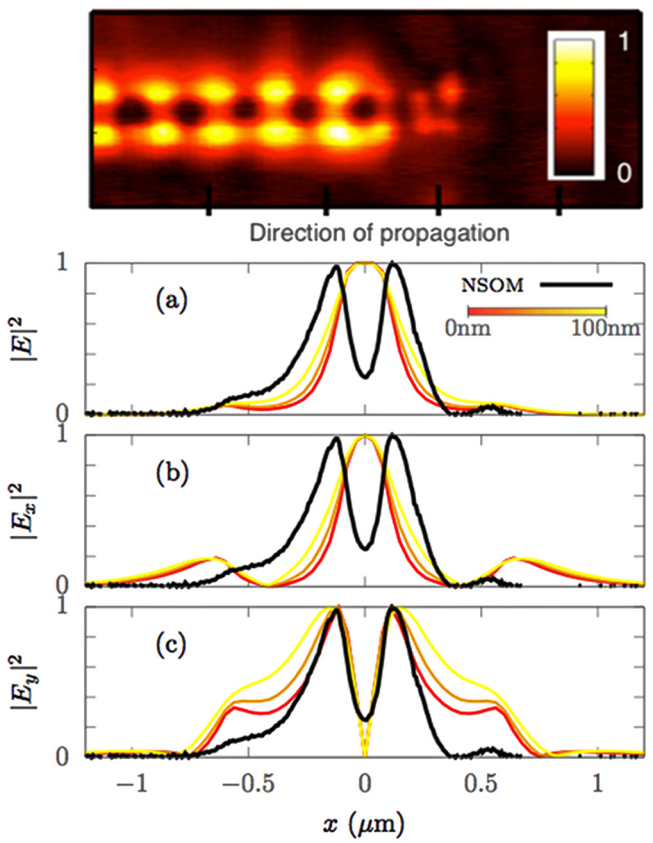

FIG. 4. Optical near field image of the gap mode demodulated at $2f_0$ (window size is 4.5 μm). Calculated surface profiles of (a) the total E-field, (b) x-, and (c) y-components. The color lines are for profiles at $y = 20$, 45, and 100 nm. A measured profile, perpendicular to the direction of propagation, is plotted for comparison.

taken at different heights. The same observation is valid for the x-component (Fig. 4(b)). However, one can observe that the valley around $x = 0$ in the calculated y-component of the E-field at $y = 20$ nm fairly matches the experimental profile even if there is no probe included in the calculations. Another interesting point in Fig. 4 is that the experimental profile is not symmetrical. This asymmetry is a consequence of the propagation of higher-order modes in the waveguide.[21] Particularly, the linear superposition of the quasi-TE and -TM modes produces an asymmetry in the y-component of the field profile that depends on their excitation weight.

In summary, a vertically integrated plasmonic nanogap waveguide on silicon has been fabricated and characterized with a perturbation-NSOM. A quantitative analysis of the coupler was obtained via the application of the strongly coupled-mode theory. In conclusion, the signal measured in the perturbation-NSOM is proportional to the local optical power scattered by the main axis of the probe and it is normalized to the local optical power carried. The vertical oscillation of the probe results in a modulation of the detected signal; however, the main contribution to the NSOM signal comes from the scattering near the surface of the sample where the evanescent field is significant. The lock-in amplifier increases the signal-to-noise ratio and allows us to measure the harmonics of the optical signal. The high coupling efficiency of the coupler is the result of a large mode overlap. Such efficient integrated plasmonic nanogap waveguides open the door to further investigations.

This work has been supported by the Agence Nationale pour la Recherche under the contract Placido ANR-08-BLAN-0285-01. A.A.'s grant has been partially funded by Region Champagne Ardenne. R.S.M. thanks William T. Snider from Texas A&M University for fruitful discussions.

[1]N. Djaker, R. Hostein, E. Devaux, T. W. Ebbesen, and H. Rigneault, and J. Wenger, J. Phys. Chem. C **114**, 16250 (2010).
[2]P. Debackere, S. Scheerlinck, P. Bienstman, R. Baets, Opt. Express **14**, 7063 (2006).
[3]J. Dionne, L. Sweatlock, M. Sheldon, A. Alivisatos, and H. Atwater. IEEE J. Sel. Top. Quantum Electron. **16**(1), 295–306 (2010).
[4]A. A. Reiserer, J.-S. Huang, B. Hecht, and T. Brixner. Opt. Express **18**(11), 11810–11820 (2010).
[5]D. K. Gramotnev and S. I. Bozhevolnyi, Nat. Photonics **4**, 83 (2010).
[6]J. Wen, S. Romanov, and U. Peschel, Opt. Express **17**, 5925 (2009).
[7]J. Wen, P. Banzer, A. Kriesch, D. Ploss, B. Schmauss, and U. Peschel, Appl. Phys. Lett. **98**, 101109 (2011).
[8]J. Tian, S. Yu, W. Yan, and M. Qiu, Appl. Phys. Lett. **95**, 013504 (2009).
[9]C. Delacour, S. Blaize, P. Grosse, J.-M. Fedeli, A. Bruyant, R. Salas-Montiel, G. Lerondel, and A. Chelnokov, Nano Lett. **10**, 2922 (2010).
[10]J. Nelayah, M. Kociak, O. Stephan, F. J. Garcia de Abajo, M. Tence, L. Henrard, D. Taverna, I. Pastoriza-Santos, L. M. Liz-Marzan, and C. Colliex. Nat. Phys. **3**(5), 348353 (2007).
[11]M. Esslinger, J. Dorfmuller, W. Khunsin, R. Vogelgesang, and K. Kern. Rev. Sci. Instrum. **83**(3), 033704 (2012).
[12]M. Schnell, A. Garcia-Etxarri, A. J. Huber, K. B. Crozier, A. Borisov, J. Aizpurua, and R. Hillenbrand, J. Phys. Chem. C **114**(16), 7341–7345 (2010).
[13]S. Bourzeix, J. M. Moison, F. Mignard, F. Barthe, A. C. Boccara, C. Licoppe, B. Mersali, M. Allovon, and A. Bruno, Appl. Phys. Lett. **73**, 1035 (1998).
[14]J.-C. Weeber, Y. Lacroute, and A. Dereux, Phys. Rev. B **68**, 115401 (2003).
[15]F. Gesuele, C. X. Pang, G. Leblond, S. Blaize, A. Bruyant, P. Royer, R. Deturche, P. Maddalena, and G. Lerondel, Physica E (Amsterdam) **41**, 1130 (2009).
[16]S. Tascu, P. Moretti, S. Kostritskii, and B. Jacquier, Opt. Mater. **24**, 297 (2003).
[17]W. C. L. Hopman, R. Stoffer, and R. M. de Ridder, J. Lightwave Technol. **25**, 1811 (2007).
[18]K. Foubert, L. Lalouat, B. Cluzel, E. Picard, D. Peyrade, E. Delamadeleine, F. de Fornel, and E. Hadji, Appl. Phys. Lett. **93**, 251103 (2008).
[19]R. M. de Ridder, W. C. L. Hopman, and E. J. Klein, "Characterization techniques for planar optical microresonators" *Photonic Crystals: Physics and Technology*, edited by C. Sibilia, T. M. Benson, M. Marciniak, and T. Szoplik (Springer, Milano, Italy, 2008), pp. 193–216.
[20]J. T. Robinson, S. F. Preble, and M. Lipson, Opt. Express **14**, 10588 (2006).
[21]R. Salas-Montiel, S. Blaize, A. Bruyant, A. Apuzzo, G. Lerondel, C. Delacour, P. Grosse, J.-M. Fedeli, and A. Chelnokov, Proc. SPIE **7943**, 79430R (2011).
[22]S.-L. Chuang, J. Lightwave Technol. **5**, 5 (1987).
[23]S.-L. Chuang, IEEE J. Quantum Electron. **23**, 499 (1987).
[24]R. Salas-Montiel, A. Apuzzo, A. Bruyant, P. Royer, G. Lerondel, and S. Blaize, Proc. SPIE **7943**, 79430S (2011).
[25]A. V. Zayats, I. I. Smolyaninov, and A. A. Maradudin, Phys. Rep. **408**, 131 (2005).